Kinematic Fitting in CLAS

M. Williams C. A. Meyer
Carnegie Mellon University, Pittsburgh, PA 15213

November 17, 2003

Abstract

We have achieved good results kinematically fitting data taken with the CLAS detector. We constructed the full covariance matrix by improving the tracking covariance matrix found in the TBER bank, while adding in energy loss and multiple scattering effects. We have been able to produce nearly flat Confidence Level distributions in the channels $\gamma p \to p\pi^+\pi^-$ and $\gamma p \to p\pi^+\pi^-\pi^o$. The pull distributions obtained from these fits are very well approximated by Gaussians with σ's ranging from 0.966 to 1.064. Kinematic quantities, such as missing mass spectra, calculated from the fit data show significant improvement over those calculated prior to fitting. Also, backgrounds can be significantly reduced.

1 Introduction

Kinematic fitting is a mathematical process that uses physical constraints, such as energy-momentum conservation, to improve measurements. In this paper, we use Lagrangian multipliers to handle the constraints while fitting using the method of least squares. We will introduce two important ways of evaluating the performance of the fits, the Confidence Level and pull distributions. The Confidence Level is used to measure the goodness-of-fit of the data to the hypothesized event. The pull distributions are used to evaluate the quality of the error estimation.

Track reconstruction in CLAS is carried out in a sector-dependent coordinate system. This coordinate system was also used while performing the kinematic fits. During tracking, a covariance matrix is produced containing the resolution errors and correlation coefficients of the tracking parameters for each track (it can be found in the TBER bank). We have found some small, but important, errors in this tracking covariance matrix which need to be corrected. The full covariance matrix can then be constructed by adding in energy loss and multiple scattering effects to the improved tracking covariance matrix. We have devised a technique which allows us to obtain good approximations for the errors in the measured quantities. The Confidence Level and pull distributions of the fits are then used to fine-tune these approximations. Once an accurate covariance matrix is constructed, the process of kinematic fitting is a fairly simple one.

After constructing the full covariance matrix, we kinematically fit the channels $\gamma p \to p\pi^+\pi^-$ and $\gamma p \to p\pi^+\pi^-\pi^o$. The Confidence Level and pull distributions of the former, which is an inclusive

channel and thus produces a 4-C fit, will be used to demonstrate the quality of the fitting. In this channel, which contains particles traveling as slow as $\beta \approx 0.35$ up to as fast as $\beta \approx 0.99$, we are able to produce a nearly flat Confidence Level distribution. The pull distributions of this channel are very well approximated by Gaussians with σ's ranging from 0.966 to 1.064. The latter channel, which contains a missing neutral particle, will be used to show how kinematic fitting can improve quantities such as missing mass spectra and reduce backgrounds.

2 Least Squares Fitting

2.1 The Method of Lagrangian Multipliers [1]

In this section, we look at the general case of least squares fitting using the method of Lagrangian multipliers to handle the constraint equations. In principle, each constraint equation could be used to eliminate one of the observed quantities. One could then proceed with a smaller set of quantities to be fit. However, we choose to instead use Lagrangian multipliers allowing us to treat each of the unknowns equally.

First we set up our notation. The m unknown parameters are put in the vector $\mathbf{x}$. The n measurable quantities are put in the vector $\mathbf{y}$. The actual measured quantities and their errors are the n-vectors $\boldsymbol{\eta}$ and $\boldsymbol{\epsilon}$ respectively. Therefore,

$$\boldsymbol{\eta} = \mathbf{y} + \boldsymbol{\epsilon}. \tag{1}$$

The vectors $\mathbf{x}$ and $\mathbf{y}$ are related by the r constraint functions

$$f_k(\mathbf{x}, \mathbf{y}) = 0, \qquad k = 1, 2, ..., r. \tag{2}$$

We assume we have a first approximation of the unknowns $\boldsymbol{x_0}$. We take $\boldsymbol{y_0} = \boldsymbol{\eta}$ and require that the constraint functions be well approximated by linear functions in the neighborhood around $(\boldsymbol{x_0}, \boldsymbol{y_0})$ determined by $\boldsymbol{x} - \boldsymbol{x_0}$ and $\boldsymbol{y} - \boldsymbol{y_0}$. We can then Taylor expand, to first order, the constraint functions in that neighborhood yielding

$$\begin{aligned} f_k(\mathbf{x}, \mathbf{y}) \;=\; & f_k(\mathbf{x_0}, \mathbf{y_0}) \;+\; \left(\frac{\partial f_k}{\partial x_1}\right)_{\mathbf{x_0},\mathbf{y_0}} (x_1 - x_{1_0}) \;+\; \ldots \;+\; \left(\frac{\partial f_k}{\partial x_m}\right)_{\mathbf{x_0},\mathbf{y_0}} (x_m - x_{m_0}) \\ & +\; \left(\frac{\partial f_k}{\partial y_1}\right)_{\mathbf{x_0},\mathbf{y_0}} (y_1 - y_{1_0}) \;+\; \ldots \;+\; \left(\frac{\partial f_k}{\partial y_n}\right)_{\mathbf{x_0},\mathbf{y_0}} (y_n - y_{n_0}). \end{aligned} \tag{3}$$

It is then convenient to introduce the matrices,

$$a_{ij} = \left(\frac{\partial f_i}{\partial x_j}\right)_{\mathbf{x_0},\mathbf{y_0}}, \qquad A = \begin{pmatrix} a_{1,1} & a_{1,2} & \ldots & a_{1,m} \\ a_{2,1} & a_{2,2} & \ldots & a_{2,m} \\ \vdots & \vdots & \ddots & \vdots \\ a_{r,1} & a_{r,2} & \ldots & a_{r,m} \end{pmatrix}, \tag{4}$$

$$b_{ij} = \left(\frac{\partial f_i}{\partial y_j}\right)_{\mathbf{x_0},\mathbf{y_0}}, \qquad B = \begin{pmatrix} b_{1,1} & b_{1,2} & \ldots & b_{1,n} \\ b_{2,1} & b_{2,2} & \ldots & b_{2,n} \\ \vdots & \vdots & \ddots & \vdots \\ b_{r,1} & b_{r,2} & \ldots & b_{r,n} \end{pmatrix}, \tag{5}$$

and the vectors,

$$c_k = f_k(\mathbf{x_0}, \mathbf{y_0}), \qquad \mathbf{c} = \begin{pmatrix} c_1 \\ c_2 \\ \vdots \\ c_r \end{pmatrix}, \tag{6}$$

$$\boldsymbol{\xi} = \mathbf{x} - \mathbf{x_0}, \qquad \boldsymbol{\delta} = \mathbf{y} - \mathbf{y_0}. \tag{7}$$

Using (4)-(7), we can now rewrite (3) as

$$A\boldsymbol{\xi} + B\boldsymbol{\delta} + \mathbf{c} = 0. \tag{8}$$

Since this is a least squares fit, we want to minimize the quantity $\boldsymbol{\delta}^T C_\eta^{-1} \boldsymbol{\delta}$, where C_η is the covariance matrix of the measured quantities. In the case where the η_j's are independent measurements, the quantity $\boldsymbol{\delta}^T C_\eta^{-1} \boldsymbol{\delta}$ takes on the more familiar form of $\sum_{j=1}^{n} \frac{\epsilon_j^2}{\sigma_j^2}$.

We now introduce the Lagrangian,

$$L = \boldsymbol{\delta}^T C_\eta^{-1} \boldsymbol{\delta} + 2\boldsymbol{\mu}^T (A\boldsymbol{\xi} + B\boldsymbol{\delta} + \mathbf{c}), \tag{9}$$

where $\boldsymbol{\mu}$ is the r-vector of Lagrangian multipliers. Setting the total differential of L equal to zero yields

$$\frac{\partial L}{\partial \boldsymbol{\delta}} = \frac{\partial L}{\partial \boldsymbol{\xi}} = 0, \tag{10}$$

since $\boldsymbol{\delta}$ and $\boldsymbol{\xi}$ are independent variables. Substituting the solutions of (10) into (8) we get

$$\boldsymbol{\xi} = -(A^T C_B A)^{-1} A^T C_B \mathbf{c}, \tag{11}$$

and the least squares estimation of the deviations

$$\boldsymbol{\delta} = -C_\eta B^T C_B (\mathbf{c} - A(A^T C_B A)^{-1} A^T C_B \mathbf{c}), \tag{12}$$

where C_B is defined as $(BC_\eta B^T)^{-1}$. Using (11) and (12), we can now write the least squares estimates for the parameters $\mathbf{x}$ and improved measurements $\mathbf{y}$ as

$$\mathbf{x} = \mathbf{x_0} + \boldsymbol{\xi}, \tag{13}$$

$$\mathbf{y} = \mathbf{y_0} + \boldsymbol{\delta}. \tag{14}$$

When the constraint equations are nonlinear, these results should be considered as better approximations and the process iterated. This is done by replacing $\mathbf{x_0}$ and $\mathbf{y_0}$ in (4)-(7) by the fit results for $\mathbf{x}$ and $\mathbf{y}$. The iteration process can be carried out until the solution obtained is satisfactory.

We can then write the least squares measurement error estimates as the n-vector

$$\boldsymbol{\epsilon} = \boldsymbol{\eta} - \mathbf{y}, \tag{15}$$

where the y_j's are the improved measurements obtained form the final iteration and the η_j's are the measured values. If the errors are normally distributed and the constraint functions are sufficiently linear around $(\boldsymbol{x_0}, \boldsymbol{y_0})$, then $\boldsymbol{\epsilon}^T C_\eta^{-1} \boldsymbol{\epsilon}$ follows a χ^2 distribution with r - m degrees of freedom.

Finally, we can use propagation of errors to write the covariance matrix for the improved measurements as

$$C_y = C_\eta - C_\eta B^T C_B B C_\eta + C_\eta B^T C_B A (A^T C_B A)^{-1} A^T C_B B C_\eta. \tag{16}$$

2.2 Confidence Levels and Pull Distributions [2]

After performing the fit, we need a way to check the agreement between the data and the hypothesis. The primary measure of the goodness-of-fit of an event is the Confidence Level. The Confidence Level of a fit result is defined as,

$$CL = \int_{\chi^2}^{\infty} f(z;n)dz \ , \tag{17}$$

where $f(z;n)$ is the χ^2 probability density function with n degrees of freedom(where we assume normally distributed errors). It is a measure of the probability that a χ^2 from the theoretical distribution is greater than the χ^2 obtained from the fit. Values for the Confidence Level can be obtained from the CERNLIB routine PROB, or in ROOT by calling the function TMath::Prob(chisq,ndf).

In the absence of background, the Confidence Level follows a flat distribution ranging from 0 to 1. Background events, those that do not satisfy the hypothesized constraint equations, produce a sharp rise near zero Confidence Level. Cutting out events with low Confidence Level provides a controlled and understandable way to eliminate the majority of the background while losing a well defined amount of the signal.

To effectively use the Confidence Level to cut background, a good understanding of each fit quantity's errors (systematic and resolution) is needed. The quality of the error estimation can be obtained by examining the Pull Distributions, also called "stretch functions". The Pull of the i^{th} fit quantity is defined as,

$$z_i = \frac{\epsilon_i}{\sigma(\epsilon_i)} \ , \tag{18}$$

where $\epsilon_i = \eta_i - y_i$ with standard deviation σ_{ϵ_i}. We write the pulls in terms of $\boldsymbol{\epsilon}$ because it is the only quantity for which the true mean value of each measurement is known. Substituting in for σ_{ϵ_i}, we can write the i^{th} pull as,

$$z_i = \frac{\eta_i - y_i}{\sqrt{\sigma^2(\eta_i) - \sigma^2(y_i)}} \ . \tag{19}$$

The z_i's should be normally distributed about zero with $\sigma = 1$. A systematic error in one of the measured quantities, η_i, can be seen as an overall shift in the distribution of the corresponding z_i away from zero. Similarly, if the error of η_i has been consistently (overestimated) underestimated, then the corresponding Pull distribution will be too (narrow) broad. Also, it is possible to parameterize the errors incorrectly but have a flat Confidence Level distribution. The pull distributions provide a way to guard against this.

3 Track Reconstruction in CLAS

Before discussing momentum corrections and kinematic fitting, we must first cover how tracking is performed in CLAS. This section deals with the coordinate system used and the covariance matrix produced during track reconstruction. The tracking parameters will also be introduced. We will show how the tracking system relates to the more familiar lab system and evaluate the tracking covariance matrix.

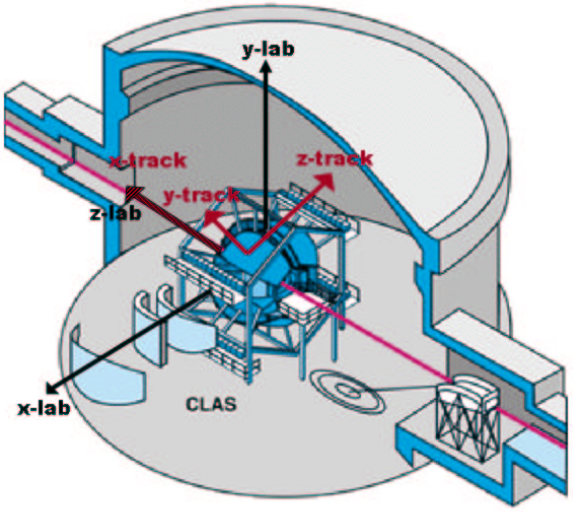

Figure 1: The lab coordinate system along with the tracking coordinates for sector 2 [3].

3.1 Coordinate Systems [4]

Track reconstruction in CLAS is carried out in a sector-dependent coordinate system. In the tracking coordinate system, the x_{track}-axis lies along the beam line, the y_{track}-axis passes through the center of the sector and the z_{track}-axis is aligned with the average magnetic field direction in that sector (see fig.1). Therefore, the tracking coordinates are related to the lab coordinates by,

$$\begin{pmatrix} x_{track} \\ y_{track} \\ z_{track} \end{pmatrix} = \begin{pmatrix} z_{lab} \\ cos(\alpha)x_{lab} + sin(\alpha)y_{lab} \\ -sin(\alpha)x_{lab} + cos(\alpha)y_{lab} \end{pmatrix}, \tag{20}$$

where $\alpha = \frac{\pi}{3}(N_{sector} - 1)$.

The tracking parameters are q/p, λ, ϕ, D_0 and Z_0. The latter two are used in vertex reconstruction but were not used in kinematic fitting and will not be discussed here. The parameter q is the charge of the particle, p is the particle's momentum in the lab frame, λ is the dipolar angle relative to the sector's (x_{track}, y_{track}) plane ($\lambda \epsilon (-\frac{\pi}{6}, \frac{\pi}{6})$) and ϕ is the angle in the sector's (x_{track}, y_{track}) plane relative to the x_{track}-axis. The track parameters along with the covariance matrix for each track can be found in the TBER bank.

Using the tracking coordinates, we can then write the momentum in the lab frame as

$$\begin{pmatrix} p_{x_{lab}} \\ p_{y_{lab}} \\ p_{z_{lab}} \end{pmatrix} = \begin{pmatrix} p(cos(\lambda)sin(\phi)cos(\alpha) - sin(\lambda)sin(\alpha)) \\ p(cos(\lambda)sin(\phi)sin(\alpha) + sin(\lambda)cos(\alpha)) \\ p\ cos(\lambda)cos(\phi) \end{pmatrix}. \tag{21}$$

It was necessary to use the tracking system while performing the kinematic fits so that the correlation coefficients and resolution errors of the fit parameters could be obtained.

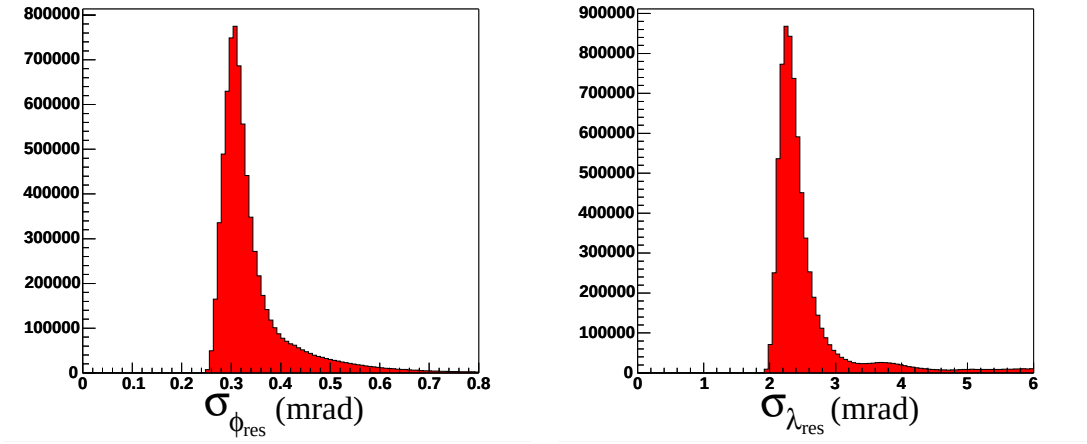

(a) (b)

Figure 2: Resolution errors found in the TBER bank for the tracking angles ϕ and λ in miliradians. Fine-tuning performed during kinematic fitting suggests these values are too small by a factor of about 1.5.

3.2 The Tracking Covariance Matrix

It is important to note that the covariance matrix found in the TBER bank is determined from tracking information only. It does not include the effects of multiple scattering or energy loss in projecting back to the vertex. The particle experiences these effects prior to reaching the tracking region of CLAS. We will address these issues later on, for now we're only interested in the resolution errors of the fit parameters and the correlation coefficients.

When performing kinematic fitting, it is very important to have an accurate covariance matrix. Therefore, we felt it was necessary to check if the values found in the tracking covariance matrix were reasonable. First, let's consider the tracking angles, λ and ϕ. The resolution error of ϕ should be approximately given by,

$$\sigma_{\phi_{res}} \approx \frac{\sigma_s}{R}, \tag{22}$$

where σ_s is the spatial resolution of the detector in the plane of ϕ and R is the distance from the track vertex to the drift chambers. Using (22) with a spatial resolution of approximately 200 μm and an average distance to the region one drift chambers of about 75 cm, we expect $\sigma_{\phi_{res}} \approx 0.27 mrad.$ Similarly, we expect $\sigma_{\lambda_{res}}$ to be about an order of magnitude bigger due to worse spatial resolution. The values found in the TBER bank for σ_ϕ^{res} and σ_λ^{res} are in good agreement with these estimates (fig.2). However, when performing the kinematic fits we found each of these values to be too small by a factor of 1.5. Therefore we adjusted the angular resolution errors according to,

$$\sigma_{\phi_{res}} = 1.5\ \sigma_{\phi_{TBER}}\ , \tag{23}$$

$$\sigma_{\lambda_{res}} = 1.5\ \sigma_{\lambda_{TBER}}\ , \tag{24}$$

where $\sigma_{\phi_{TBER}}$ and $\sigma_{\lambda_{TBER}}$ are the angular resolution errors found in the TBER bank. This results in an average resolution for ϕ (which is closely related to θ in the lab coordinate system) of about 0.48 $mrad$ and an average resolution for λ (which is closely related to ϕ in the lab coordinate system) of about 3.5 $mrad$. This translates into a reasonable average spatial resolution in the plane of ϕ of about $300\mu m$.

Tracking is performed using the quantity q/p, however, it is easier to include the energy loss effects if we fit in terms of p. Therefore, we adjusted the covariance matrix according to,

$$C_{\eta}^{pp} = \left(\frac{\partial p}{\partial(q/p)}\right)^2 C_{\eta}^{\frac{q}{p}\frac{q}{p}} = \frac{p^4}{q^2}\, C_{\eta}^{\frac{q}{p}\frac{q}{p}} \ , \tag{25}$$

$$C_{\eta}^{p\phi} = \left(\frac{\partial p}{\partial(q/p)}\right)\left(\frac{\partial \phi}{\partial \phi}\right) C_{\eta}^{\frac{q}{p}\phi} = -\frac{p^2}{q}\, C_{\eta}^{\frac{q}{p}\phi} \ , \tag{26}$$

$$C_{\eta}^{p\lambda} = \left(\frac{\partial p}{\partial(q/p)}\right)\left(\frac{\partial \lambda}{\partial \lambda}\right) C_{\eta}^{\frac{q}{p}\lambda} = -\frac{p^2}{q}\, C_{\eta}^{\frac{q}{p}\lambda} \ , \tag{27}$$

where p is the measured momentum of the particle.

Evaluating the resolution error of p isn't as easy as for λ and ϕ, but we can make some general arguments about its dependence on p and θ (the polar angle in the lab system). First, we know that $\sigma_{p_{res}}$ must increase as p increases (tracks with higher momentum bend less which leads to worse resolution). Furthermore, tracking a particle through a magnetic field generally results in σ_p/p being linear in p. The resolution must also depend on $\int \vec{B} \cdot \vec{dl}$, the amount of magnetic field the particle travels through. The toroidal field produced in CLAS is approximately azimuthally uniform, however, it has a strong θ dependence. Figure 3 clearly shows the strength of the magnetic field is greater in the forward direction and decreases as θ increases. Therefore, $\sigma_{p_{res}}$ must increase with θ.

Figure 5 shows the values of $\sigma_{p_{res}}/p$ taken from the TBER bank are in fact linear in p and have the θ-dependence described above. However, when performing the kinematic fits, we found that the overall magnitude of $\sigma_{p_{res}}$ appeared to be too small by a factor of 2. Coincidently, the torus current for the runs we are examining was approximately $I_{max}/2$. If the errors found in the TBER bank do not account for the actual torus current, then they would be off by a factor of I_{max}/I (since the toroidal field is linear in I). For the g1c run period this appears to be the case. So we adjusted the momentum errors according to,

$$\sigma_{p_{res}} = \frac{I_{max}}{I}\, \sigma_{p_{TBER}} \ , \tag{28}$$

where $I_{max} = 3860A$, I is the actual torus current in amps and $\sigma_{p_{TBER}}$ is the standard deviation of p found in the TBER bank. We end the discussion on $\sigma_{p_{res}}$ by noting that all of the runs we have analyzed have $I \simeq 1920A$, so we can't be sure if neglecting the actual torus current is the reason for the discrepancy in $\sigma_{p_{TBER}}$, however, it seems to be the most likely explanation.

The correlation coefficients appear to be reasonable. They show a strong correlation between q/p and ϕ as expected (recall that ϕ is closely related to θ in the lab system). All other correlations are relatively weak, which is also what we would expect (see fig.4).

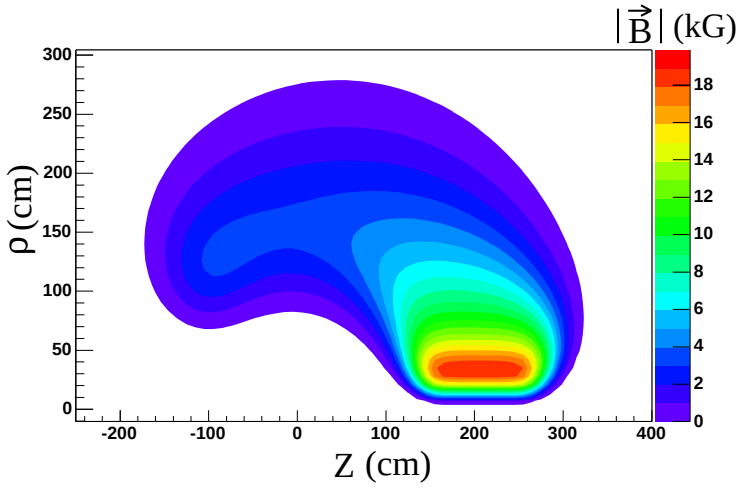

Figure 3: The magnitude of the toroidal magnetic field, at full current, in kilogauss. Z is the beam direction and ρ is the distance from the beam line in cylindrical coordinates. The strong θ dependence of the field is clearly evident.

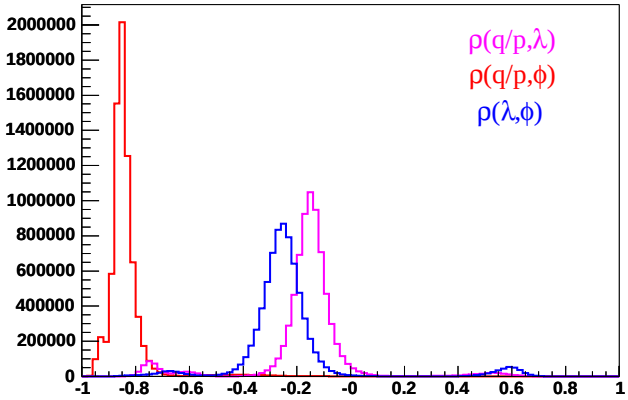

Figure 4: Correlation coefficients for the tracking parameters $\frac{q}{p}, \lambda, \phi$. There is a strong correlation between q/p and ϕ, $\rho(q/p, \phi) \approx -0.85$. The correlations between the other tracking parameters are fairly weak, $\rho(q/p, \lambda) \approx -0.15$ and $\rho(\lambda, \phi) \approx -0.27$. The small bumps away from the peaks correspond to poorly measured tracks.

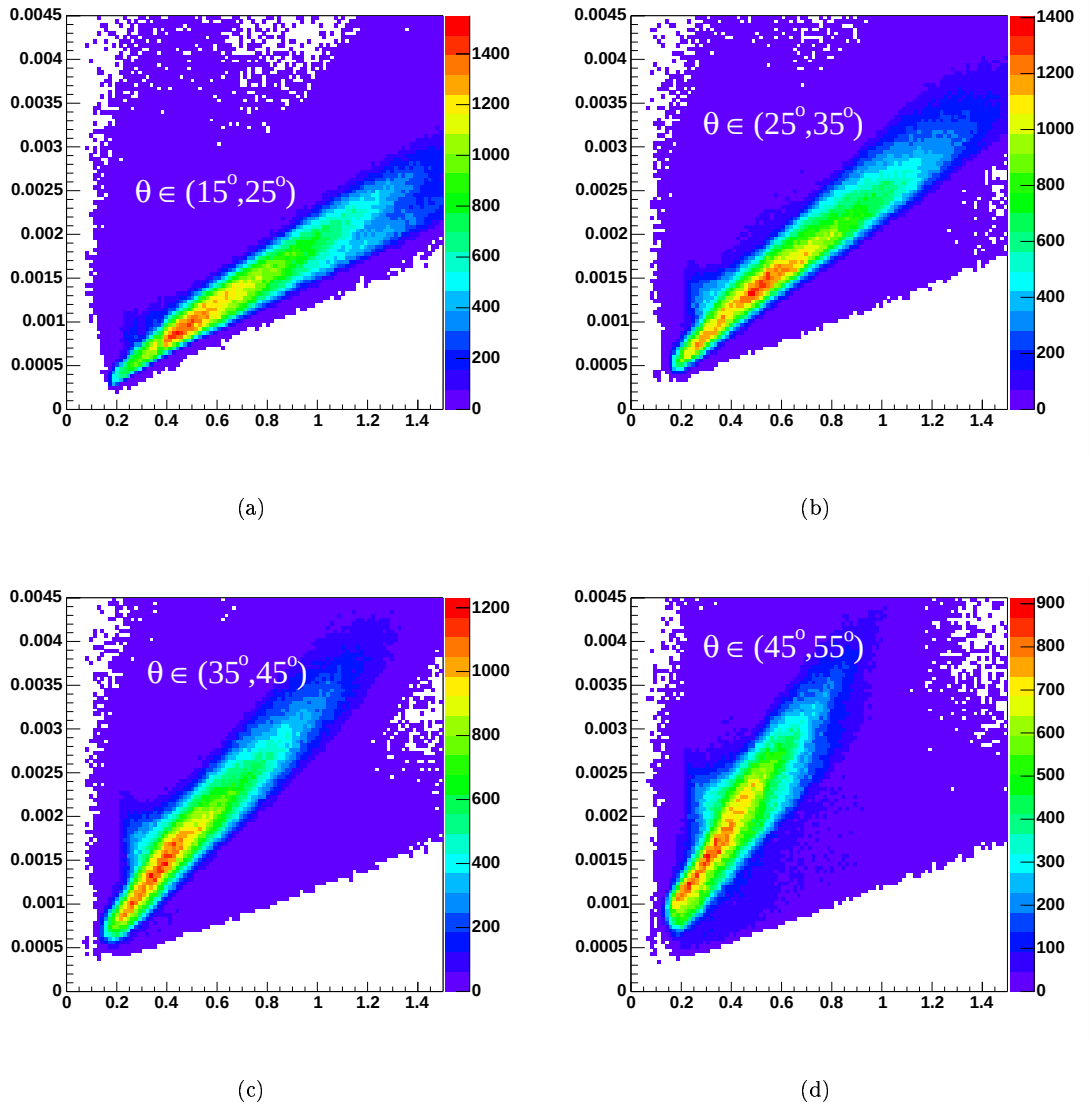

Figure 5: $\sigma_{p_{res}}/p$ vs. p : Resolution errors found in the TBER bank for the magnitude of the measured momentum for four different polar angle ranges. As expected, $\sigma_{p_{res}}/p$ is linear in p and increases with θ. Fine-tuning performed during kinematic fitting suggests the TBER bank does not account for the actual torus current. Therefore, the resolution error of the momentum must be scaled by a factor of I_{max}/I.

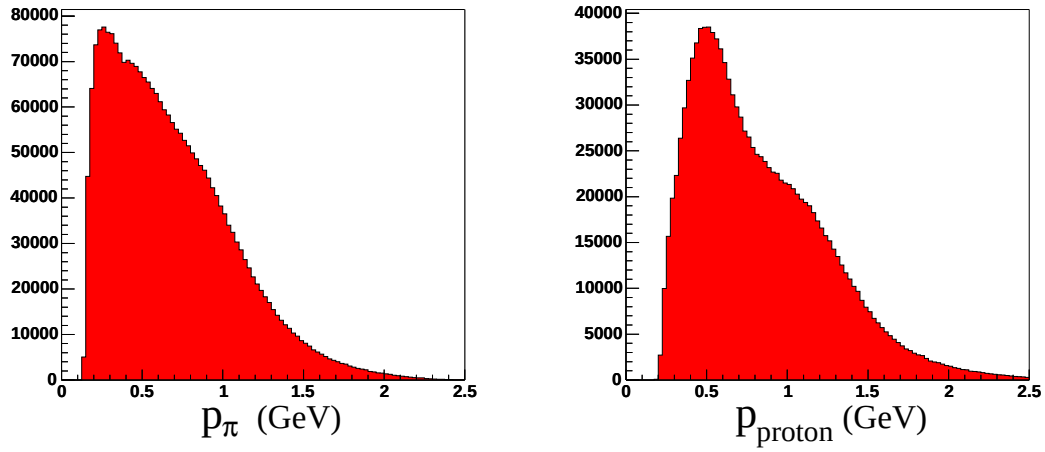

(a) (b)

Figure 6: Measured Momenta for protons and pions detected in $\gamma p \to p\pi^+\pi^- X$ events.

4 Calculating Energy Loss and Multiple Scattering Effects in CLAS

A large number of the protons detected in the g1c run period from $\gamma p \to p\pi^+\pi^- X$ events, are slow enough for energy loss and multiple scattering effects, mainly in the target and the carbon fiber beam pipe, to become important (a typical proton travels at $\beta \approx 0.7$, see fig.6b). The protons experience energy loss before they enter the drift chamber regions. Consequently, the measured momentum is smaller than the momentum the proton had leaving the interaction vertex and must be corrected. We must also consider how errors due to energy loss and multiple scattering affect the covariance matrix. Below we present an approach that allows us to calculate the mean momentum correction and to estimate the errors in the measured kinematic quantities.

To calculate the affects of energy loss and multiple scattering on the proton, we needed a clean, inclusive channel with a proton in the final state. We chose $\gamma p \to p\pi^+\pi^-$, which was then kinematically fit treating the proton as a missing particle. The fit proton was then compared to the measured proton to determine the effects of multiple scattering and energy loss. The pions are also affected by these processes, but to a much lesser degree (a typical pion travels at $\beta > 0.87$, see fig.6a). Still, energy loss and multiple scattering effects are important for pions and must be included.

To isolate the channel $\gamma p \to p\pi^+\pi^-$, we required that each of the final state particles be detected and the total missing mass squared ϵ $(-0.01, 0.01)(GeV/c^2)^2$. We also required the missing mass off the pions to be within 40 MeV of the proton mass. To help eliminate background events due to matching an event with the wrong beam photon, a cut was placed on the missing momentum in the beam direction of $|p^z_{missing}| < 0.05\ GeV/c$ [5]. Fiducial volume cuts were also applied to eliminate events containing particles whose trajectories took them through regions of CLAS where

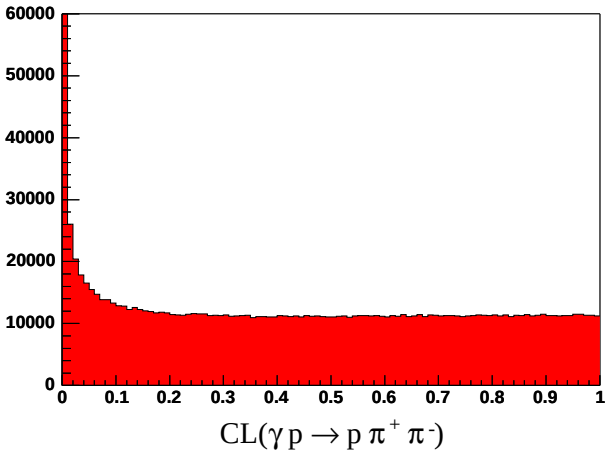

Figure 7: Confidence Level distribution for $\gamma p \to p\pi^+\pi^-$ events treating the proton as a missing particle (a 1-C fit).

the resolution is significantly decreased due to shadowing caused by the toroidal coils. Finally, after the kinematic fit was performed with the missing proton, we required the Confidence Level to be at least 0.1 (see fig.7). These cuts were chosen to insure that the channel was clean and because they are the standard types of cuts made on CLAS data. Later, we will show that once you have an accurate covariance matrix, only the confidence level cut is necessary.

4.1 Momentum Corrections

Momentum corrections for charged particles in photon runs at CLAS are handled by the Eloss package written by Eugene Pasyuk. This package contains all the information concerning the geometry and material of the target, the beam pipe and the start counter. Below we present an approach to calculating mean momentum corrections that requires almost no information about what the particle passes through prior to reaching the tracking region of CLAS. We present this technique as a quick way to calculate fairly accurate momentum corrections for runs where the Eloss package is not available. The Eloss package should be used when available (for all photon runs), the main goal of this section is to demonstrate that some form of momentum corrections must be applied prior to any fitting.

This section is meant to demonstrate how kinematic fitting could be used to correct measured momenta. We do not consider vertex positions, which is something that must be done if this technique were to be used in data analysis. We can not expect to reproduce the accuracy of the Eloss package, however, the results suggest that the corrections it produces differ from those of the Eloss package by only about 10% of the correction (for particles that orginate far enough from the edges of the target for vertex information to be of little importance). Hopefully this section will show how important momentum corrections are, especially for slow protons.

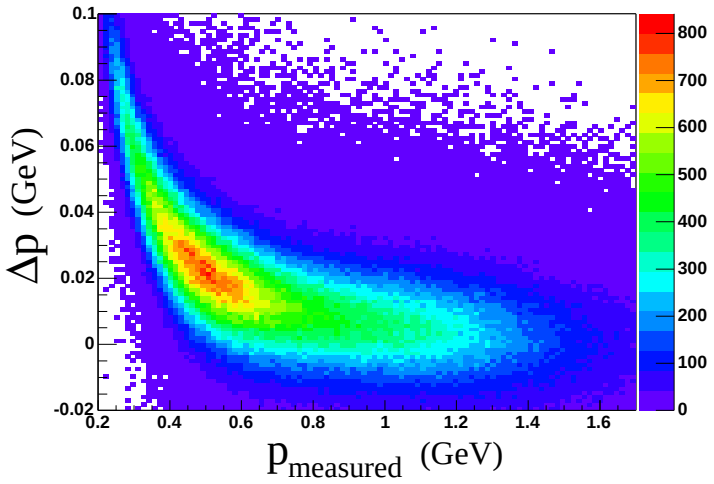

Figure 8: $p_{fit} - p_{measured}$ vs. $p_{measured}$: comparing measured proton momenta to fit results. Clearly, some type of momentum correction must be applied.

First we consider the path length, x, of material the particle traverses. The two main sources of energy loss are presumed to be the target and the carbon-fiber beam pipe. Both are cylindrical, therefore $x \propto 1/sin(\theta)$. Figure 8 shows the results of comparing p_{fit} and $p_{measured}$ for protons. As expected, the energy lost increases as $p_{measured}$ decreases. We can parameterize the momentum correction as,

$$\Delta p_{proton} = \left(\frac{A}{p} + \frac{B}{p^2} + \frac{C}{p^3} + \frac{D}{p^4} \right) \frac{1}{sin(\theta)} , \tag{29}$$

where p is the measured momentum of the proton and θ is the proton's polar angle in the lab system. Figure 9 shows the results of fitting each momentum bin of Δp vs. p in 2 polar angle regions to a Gaussian, then histogramming the mean along with a plot of (29).

Generalizing this result so that it can be applied to all charged particles gives us,

$$\Delta p = \left(\frac{m}{m_p} \right)^2 \left(\frac{A}{p} + \left(\frac{m}{m_p} \right) \frac{B}{p^2} + \left(\frac{m}{m_p} \right)^2 \frac{C}{p^3} + \left(\frac{m}{m_p} \right)^3 \frac{D}{p^4} \right) \frac{1}{sin(\theta)} , \tag{30}$$

where m is the mass of the particle, m_p is the mass of the proton and p is the measured momentum of the particle. And of course,

$$p_{corrected} = p_{measured} + \Delta p . \tag{31}$$

A comparison of the results of this approach to using the Eloss package can be seen in figure 10. The agreement between the two methods is quite good (they differ by about 10% of the correction for particles that originate far enough from the edges of the target for vertex positions to be important), especially considering this method required only a very simple paramaterization of the path length through the material . The Eloss package is presumed to be more accurate do to all the factors it considers, and it was used to produce the results of all subsequent sections.

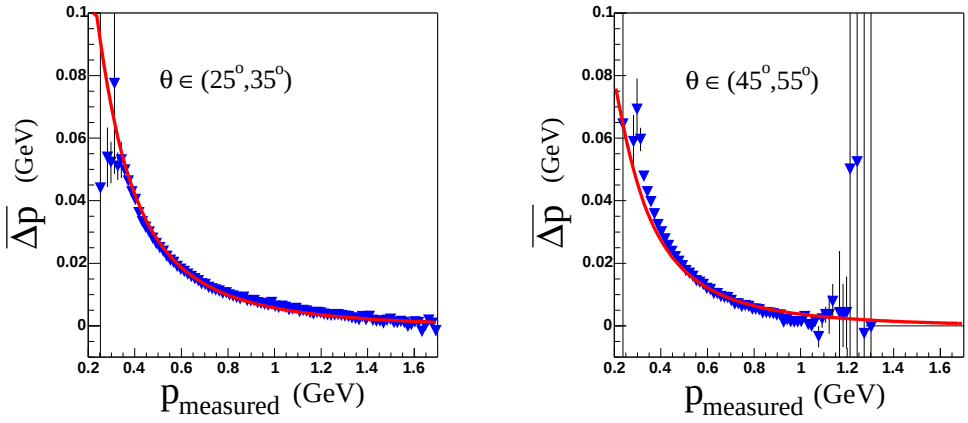

(a) (b)

Figure 9: Mean Momentum Corrections: The triangular markers were obtained by fitting each momentum bin in fig.8 to a Gaussian in the specified polar angle region. The line is (29) plotted with the values of the constants determined to be the best correction.

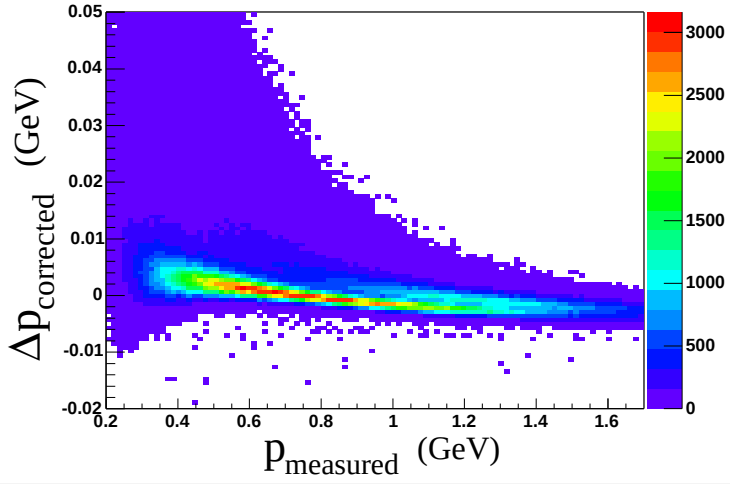

Figure 10: Comparison between corrected momenta obtained from the Eloss package and the technique discussed in section 4.1. In about 15% of the events the difference in the two corrections is greater than 10% of the correction, this is caused by the lack of vertex consideration of the technique presented in this section.

4.2 Error Estimation

The same technique, comparing the fit and measured protons, can be used to estimate the errors from multiple scattering and energy loss. For convenience, we choose to parameterize these errors in terms of the corrected momentum. It is important to note that it is impossible to entirely keep pion errors from feeding into the fit proton. The method discussed above is mainly used to obtain the functional form and a good first approximation of the errors. The Confidence Level and Pull distribution obtained from the fits must then be used to fine-tune these approximations.

Multiple scattering errors depend on the particle's path length through the material. The two main sources of multiple scattering are also presumed to be the target and the carbon fiber beam pipe giving us $x \propto 1/sin(\theta)$, where x is the path length through the material.

The full angular errors should then follow the functional form,

$$\sigma_\phi = \sqrt{\sigma^2_{\phi_{res}} + \left(\frac{\sigma_{ms}}{\beta p\sqrt{sin(\theta)}}\right)^2}\ , \tag{32}$$

$$\sigma_\lambda = \sqrt{\sigma^2_{\lambda_{res}} + \left(\frac{\sigma_{ms}}{\beta p\sqrt{sin(\theta)}}\right)^2}\ , \tag{33}$$

where p is the corrected momentum, $\sigma_{\phi_{res}}$ and $\sigma_{\lambda_{res}}$ are the angular resolution errors and σ_{ms} is a constant parameterizing the effects of multiple scattering from all the material the particle encounters prior to reaching the drift chambers.

Figure 11a shows $\Delta\phi$ *vs.* $\beta p\sqrt{sin(\theta)}$. As expected, the distribution is centered around zero and its width decreases as $\beta p\sqrt{sin(\theta)}$ increases. Each bin was fit with a Gaussian whose σ was then histogrammed as can be seen in figure 11b. The value of σ_{ms} was fine-tuned using the Confidence Level and Pull distributions of the kinematic fits performed below. A plot of (32) using the value of σ_{ms} used in the kinematic fits can be seen in figure 11b. The same technique was then used for λ, these results are shown in figures 11c and 11d.

For moderately relativistic particles, the error in the magnitude of the momentum due to energy loss follows the functional form [6],

$$\sigma^2_{p_{eloss}} \propto \left(\frac{\gamma^2(1-\beta^2/2)}{\beta^2}\right)\ x\ , \tag{34}$$

where x is the path length of material the particle traverses. This appears to work well for particles with $\beta < 0.86$, however, it diverges as $\beta \to 1$. Therefore, a piecewise function was chosen to approximate the error in p, which is given by,

$$\sigma_p = \sqrt{\sigma^2_{p_{res}} + \left(\frac{\sigma_{el}\gamma\sqrt{1-\beta^2/2}}{\beta\sqrt{sin(\theta)}}\right)^2} \qquad \text{if } \beta < 0.86\ , \tag{35}$$

$$\sigma_p = \sqrt{\sigma^2_{p_{res}} + \left(\frac{1.81\sigma_{el}}{\sqrt{sin(\theta)}}\right)^2} \qquad \text{if } \beta \geq 0.86\ , \tag{36}$$

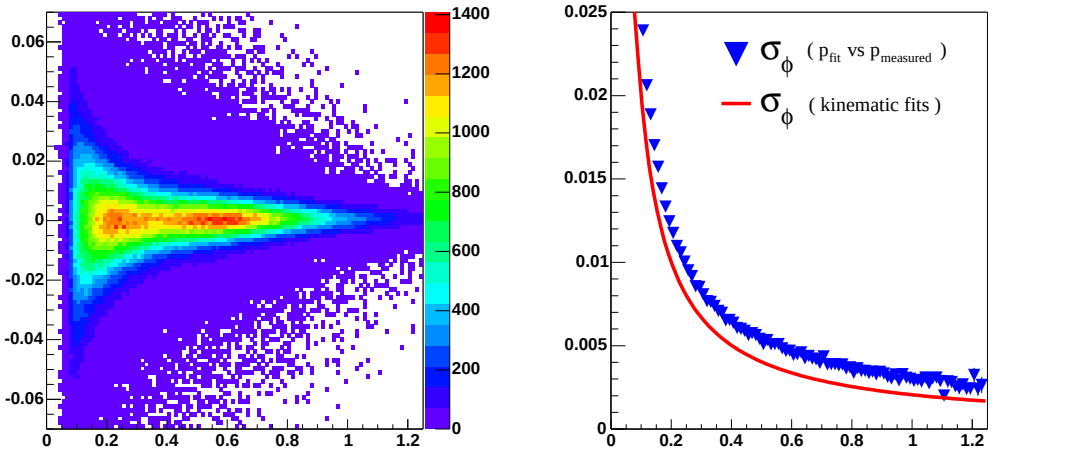

(a) (b)

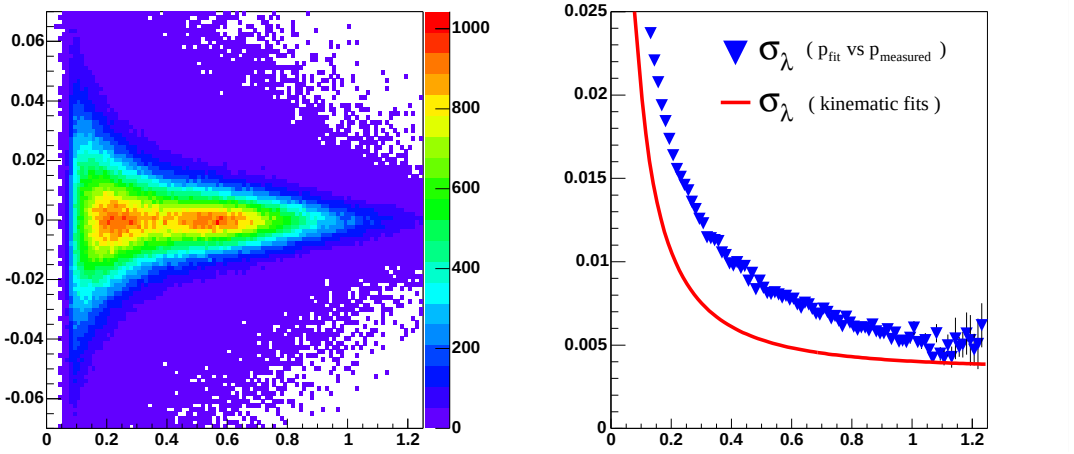

(c) (d)

Figure 11: (a) $\Delta\phi$ vs. $\beta p\ \sqrt{sin(\theta)}$: Comparing ϕ_{fit} and $\phi_{measured}$ for protons in $\gamma p \to p\pi^+\pi^-$ events fitting the proton as a missing particle. (b) σ_{phi} vs. $\beta p\ \sqrt{sin(\theta)}$: the triangular markers were obtained by fitting each bin of (a) to a Gaussian, the line represents (32) plotted with the value of σ_{ms} used in the kinematic fits. (c),(d) The same as (a),(b) but for the tracking angle λ.

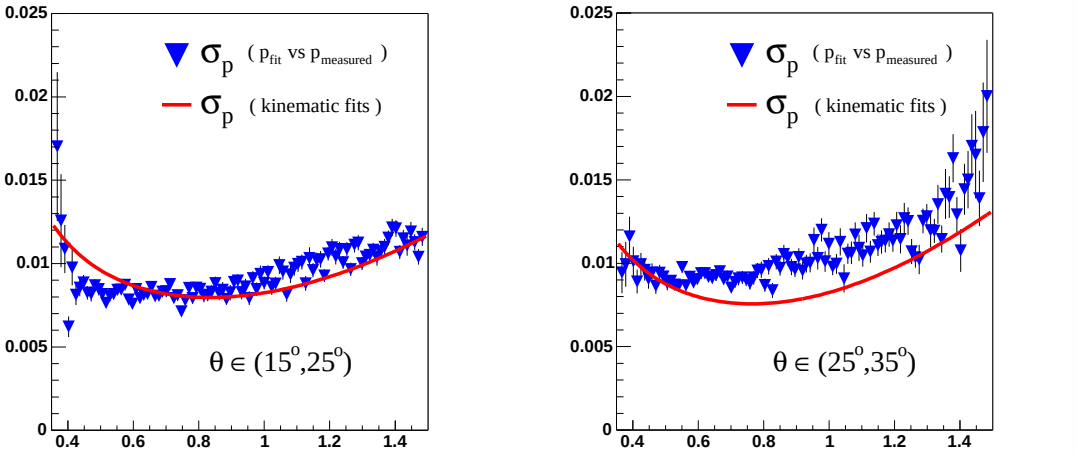

(a) (b)

Figure 12: σ_p vs. p : The triangular markers were obtained by fitting each momentum bin of fig.8 (in each figure's respective angular region) to a Gaussian, the line represents (35) plotted with the value of σ_{el} used in the kinematic fits.

where $\sigma_{p_{res}}$ is the momentum resolution error, σ_{el} is a constant parameterizing the energy loss effects and the factor of 1.81 is chosen to make the function continuous. The value of σ_{el} was also fine tuned using the Confidence Level and Pull distributions of the kinematic fits. Figure 12 shows (35) plotted with the value of σ_{el} used in the kinematic fitting for two polar angle regions along with the standard deviation in the momentum obtained by fitting each momentum bin to a Gaussian. To produce figure 12, we also placed cuts on the pion momenta of $|\vec{p_\pi}| < 0.6\ GeV$ and $\theta_\pi > 35^o$ to help limit pion momentum errors from feeding into the fit proton.

We conclude this section by discussing the error in the measurement of the tagged photon. The characteristic angle of beam photons is $m_e c^2/E_0$, where m_e is the mass of an electron and E_0 is the energy of the electron beam [7]. For the data analyzed in this paper, $E_0 = 3.115\ GeV$ which gives a characteristic angle in tagged photons of about $0.16\ mrad$. This is negligible compared to the total error in λ and ϕ (see fig.11). Therefore, the photon direction is taken to be fixed along the beam line.

Each of the 384 E-plane paddles in the tagger has an energy resolution of 0.001 E_0 [7], which for our runs is 3.115 MeV. Assuming equal acceptance along the length of each tagger paddle, gives us,

$$\sigma^2_{E_\gamma} = \frac{1}{6.230}\int_{-3.115}^{3.115} E^2 dE = 1.798\ MeV^2\ . \tag{37}$$

4.3 The Full Covariance Matrix

We are now ready to construct the full covariance matrix. To do this, we add the errors from energy loss and multiple scattering determined in section 4.2 to the diagonal elements of the improved tracking covariance matrix discussed in section 3.2. We treat energy loss and multiple scattering errors as being uncorrelated. Therefore, the off diagonal elements of the improved tracking covariance matrix are unaffected.

For an event with k charged particles in the final state, there are $3k+1$ fit parameters in the vector $\boldsymbol{\eta}$ which we can write as,

$$\boldsymbol{\eta} = \begin{pmatrix} E_\gamma \\ p_1 \\ \lambda_1 \\ \phi_1 \\ \vdots \\ p_k \\ \lambda_k \\ \phi_k \end{pmatrix} , \tag{38}$$

where E_γ is the tagged photon energy and p_i, λ_i and ϕ_i are the momentum magnitude and tracking angles of the i^{th} charged particle. The measurement of the tagged photon energy is not correlated to any other measurements. And, of course, the measurements of each charged particle's kinematic quantities are not correlated with measurements of the kinematic quantities of any other particle. Therefore, we can write the full covariance matrix for an event with k charged particles in the final state as,

$$C_\eta = \begin{pmatrix} \sigma^2_{E_\gamma} & 0 & 0 & 0 & \dots & 0 & 0 & 0 \\ 0 & C_1^{pp} & C_1^{p\lambda} & C_1^{p\phi} & \dots & 0 & 0 & 0 \\ 0 & C_1^{p\lambda} & C_1^{\lambda\lambda} & C_1^{\lambda\phi} & \dots & 0 & 0 & 0 \\ 0 & C_1^{p\phi} & C_1^{\lambda\phi} & C_1^{\phi\phi} & \dots & 0 & 0 & 0 \\ \vdots & \vdots & \vdots & \vdots & \ddots & \vdots & \vdots & \vdots \\ 0 & 0 & 0 & 0 & \dots & C_k^{pp} & C_k^{p\lambda} & C_k^{p\phi} \\ 0 & 0 & 0 & 0 & \dots & C_k^{p\lambda} & C_k^{\lambda\lambda} & C_k^{\lambda\phi} \\ 0 & 0 & 0 & 0 & \dots & C_k^{p\phi} & C_k^{\lambda\phi} & C_k^{\phi\phi} \end{pmatrix} , \tag{39}$$

where σ_{E_γ} is given in (37) and,

$$\begin{aligned} C_i^{pp} &= \left(\frac{I_{max} p_{m_i}^2}{I q_i}\right)^2 C_{TBER}^{\frac{q_i}{p_i}\frac{q_i}{p_i}} + \Theta(0.86-\beta_i)\left(\frac{0.0027 GeV \gamma_i}{\beta_i}\right)^2 \left(\frac{1-\beta_i^2/2}{sin(\theta_i)}\right) \\ &\quad + \Theta(\beta_i - 0.86)\left(\frac{2.39\times 10^{-5} GeV^2}{sin(\theta_i)}\right) , \end{aligned} \tag{40}$$

$$C_i^{\lambda\lambda} = 2.25 C_{TBER}^{\lambda_i\lambda_i} + \left(\frac{0.002 GeV\cdot rad}{\beta_i p_i \sqrt{sin(\theta_i)}}\right)^2 , \tag{41}$$

$$C_i^{\phi\phi} = 2.25 C_{TBER}^{\phi_i\phi_i} + \left(\frac{0.002 GeV\cdot rad}{\beta_i p_i \sqrt{sin(\theta_i)}}\right)^2 , \tag{42}$$

$$C_i^{p\lambda} = -\left(\frac{1.5 I_{max} p_{m_i}^2}{I q_i}\right) C_{TBER}^{\frac{q_i}{p_i}\lambda_i} , \tag{43}$$

$$C_i^{p\phi} = -\left(\frac{1.5 I_{max} p_{m_i}^2}{I q_i}\right) C_{TBER}^{\frac{q_i}{p_i}\phi_i} , \tag{44}$$

$$C_i^{\lambda\phi} = 2.25 C_{TBER}^{\lambda_i \phi_i} , \tag{45}$$

$I_{max} = 3860A$ is the maximum torus current, I is the actual torus current, p_{m_i} is the measured value of the magnitude of the i^{th} charged particle's momentum and $C_{TBER}^{a_i b_i}$ are the components of the tracking covariance matrix found in the TBER bank (values given for σ_{el} and σ_{ms} are for the g1c target).

For forward traveling particles that exit through the end of the target, a scale factor must be imposed to the energy loss and multiple scattering effects (the $1/\sin(\theta)$ parameterization of the path length is no longer valid). To do this, we use vertex information from the MVRT bank to calculate how much target material the particle actually traveled through. Then we just scale the contribution from the target material to the energy loss and multiple scattering errors. We also note that if a channel is to be fit that contains a neutral particle that decays, some care should be taken to scale the energy loss and multiple scattering effects based on the position of the secondary vertex.

Now that we have a good estimate for the covariance matrix, we will discuss two examples of kinematic fitting in CLAS.

5 Kinematic Fit of $\gamma p \rightarrow p\pi^+\pi^-$

The first step in kinematically fitting the channel $\gamma p \rightarrow p\pi^+\pi^-$ is too define our vector of fit parameters. Using notation from section 4.3, we write the vector $\boldsymbol{\eta}$ for this channel as,

$$\boldsymbol{\eta} = \begin{pmatrix} E_\gamma \\ p_p \\ \lambda_p \\ \phi_p \\ p_{\pi^+} \\ \lambda_{\pi^+} \\ \phi_{\pi^+} \\ p_{\pi^-} \\ \lambda_{\pi^-} \\ \phi_{\pi^-} \end{pmatrix} . \tag{46}$$

With this definition of $\boldsymbol{\eta}$ it is easy to construct the covariance matrix, C_η using (39)-(45). In terms of these parameters, the energy-momentum constraint functions for this channel are,

$$f_0(\mathbf{y}) = E_\gamma + m_p c^2 - \sqrt{p_p^2 c^2 + m_p^2 c^4} - \sqrt{p_{\pi^+}^2 c^2 + m_{\pi^+}^2 c^4} - \sqrt{p_{\pi^-}^2 c^2 + m_{\pi^-}^2 c^4} , \tag{47}$$

$$\begin{aligned} f_1(\mathbf{y}) \quad = \quad & p_p[cos(\lambda_p)sin(\phi_p)cos(\alpha_p) - sin(\lambda_p)sin(\alpha_p)] + p_{\pi^+}[cos(\lambda_{\pi^+})sin(\phi_{\pi^+})cos(\alpha_{\pi^+}) \\ & - sin(\lambda_{\pi^+})sin(\alpha_{\pi^+})] + p_{\pi^-}[cos(\lambda_{\pi^-})sin(\phi_{\pi^-})cos(\alpha_{\pi^-}) - sin(\lambda_{\pi^-})sin(\alpha_{\pi^-})] , \end{aligned} \tag{48}$$

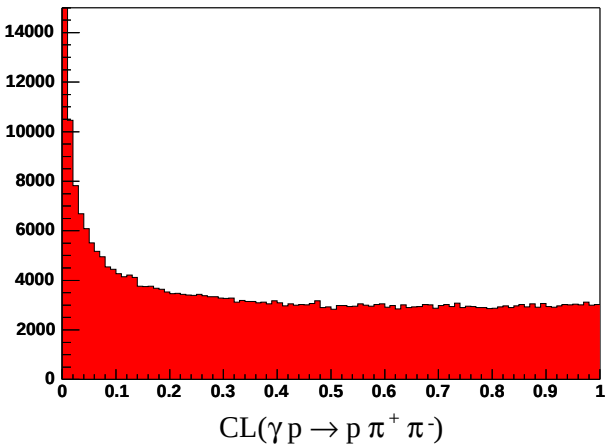

Figure 13: Confidence Level distribution obtained by kinematically fitting the channel $\gamma p \to p\pi^+\pi^-$ including the measured proton (a 4-C fit).

$$f_2(\mathbf{y}) = p_p[cos(\lambda_p)sin(\phi_p)sin(\alpha_p) + sin(\lambda_p)cos(\alpha_p)] + p_{\pi^+}[cos(\lambda_{\pi^+})sin(\phi_{\pi^+})sin(\alpha_{\pi^+}) + sin(\lambda_{\pi^+})cos(\alpha_{\pi^+})] + p_{\pi^-}[cos(\lambda_{\pi^-})sin(\phi_{\pi^-})sin(\alpha_{\pi^-}) + sin(\lambda_{\pi^-})cos(\alpha_{\pi^-})] \,, \quad (49)$$

$$f_3(\mathbf{y}) = p_p cos(\lambda_p)cos(\phi_p) + p_{\pi^+}cos(\lambda_{\pi^+})cos(\phi_{\pi^+}) + p_{\pi^-}cos(\lambda_{\pi^-})cos(\phi_{\pi^-}) - E_\gamma/c \,, \quad (50)$$

where m_p is the mass of the target proton.

We then take $\boldsymbol{y_0} = \boldsymbol{\eta}$, where the η_j's are the measured values of the fit parameters. From (47)-(50), we can then use (5) to write the matrix B in terms of $\mathbf{y_0}$. The least squares estimates of the deviations of the fit parameters can then be written as,

$$\boldsymbol{\delta} = -C_\eta B^T C_B \mathbf{c} \,, \quad (51)$$

where C_B is defined as $(BC_\eta B^T)^{-1}$ and $\mathbf{c}$ is defined in (6). The improved measurements are then written as $\boldsymbol{y} = \boldsymbol{y_0} + \boldsymbol{\delta}$. The process is iterated substituting the value obtained for $\boldsymbol{y}$ in the previous step for $\boldsymbol{y_0}$ and repeating the calculation until the solution obtained is satisfactory (any criteria enforced here to terminate the iteration process is arbitrary, we simply chose to let each event iterate 10 times). After performing the last iteration, we use $\boldsymbol{\epsilon} = \boldsymbol{\eta} - \boldsymbol{y}$ to calculate $\boldsymbol{\epsilon}^T C_\eta^{-1} \boldsymbol{\epsilon}$ which follows a χ^2 distribution with 4 degrees of freedom.

The resulting Confidence Level distribution can be seen in figure 13. As expected the distribution is nearly flat with a sharp rise near zero (recall the discussion in section 2.2). Figure 14 shows the corresponding Pull distributions, which also look like we would expect. They are each very well approximated by a Gaussian centered near zero with $\sigma \approx 1$.

The agreement between the Confidence Level and Pull distributions obtained from the fit and the theoretical distributions is quite good. This provides a high degree of confidence in the quality of the fitting and the parameterization of the errors. We also note that we have made no missing mass or momentum cuts. We simply let the fit decide whether the data matches the hypothesized

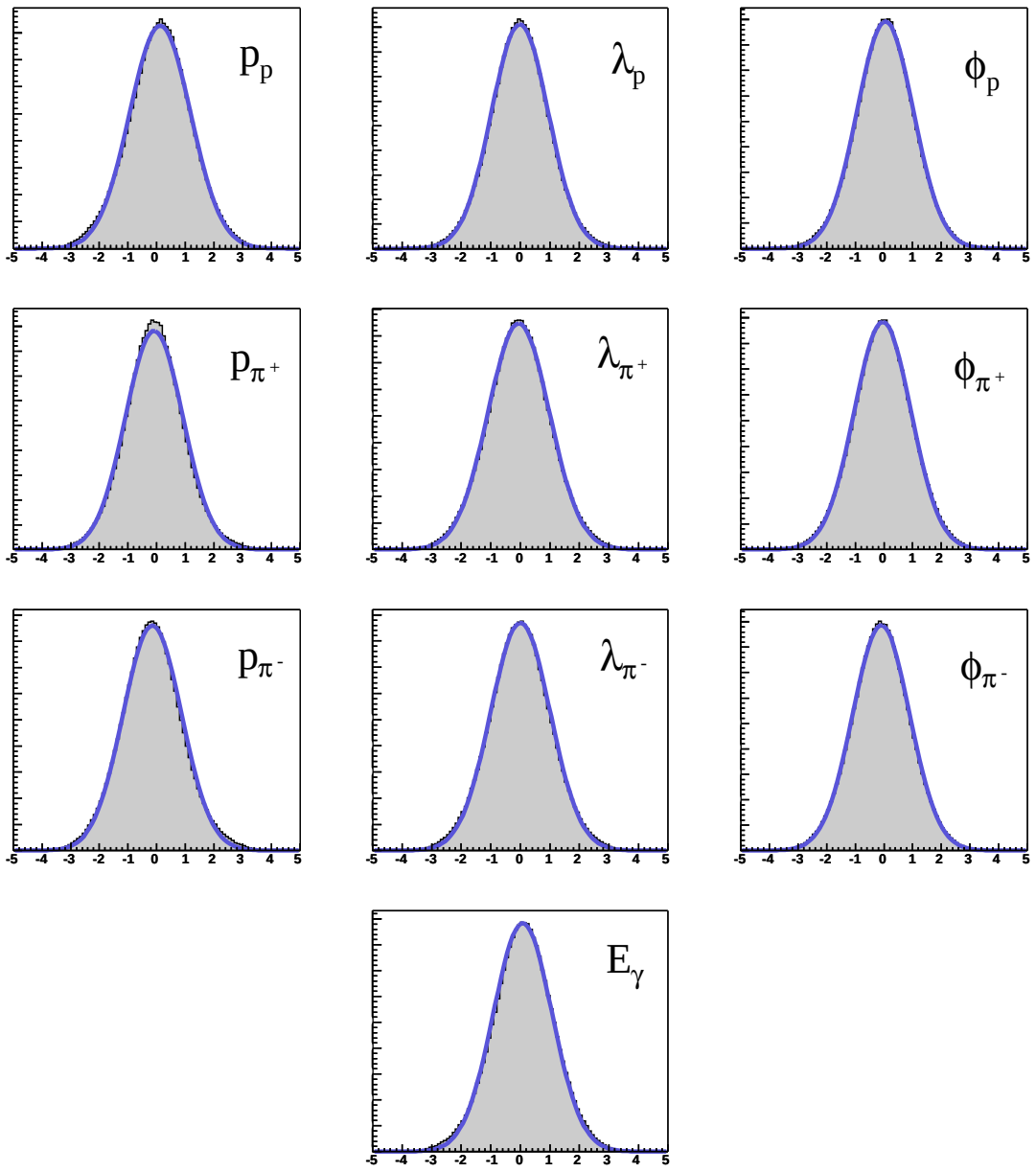

Figure 14: Pull distributions obtained from the 4-C kinematic fit of $\gamma p \to p\pi^+\pi^-$ (with a 1% Confidence Level cut applied). The line represents fitting the data to a Gaussian, the mean and σ of which can be found in table 1.

Table 1: means and σ's obtained by fitting the pull distributions of fig.14 to Guassians.

	mean	σ
p_p	0.123	1.064
λ_p	-0.015	0.966
ϕ_p	0.045	0.989
$p_{\pi+}$	-0.084	1.001
$\lambda_{\pi+}$	-0.054	1.042
$\phi_{\pi+}$	-0.045	0.999
$p_{\pi-}$	-0.149	1.020
$\lambda_{\pi-}$	0.004	1.012
$\phi_{\pi-}$	-0.097	0.998
E_γ	0.081	0.993

event. In the next section, we will show how kinematically fitting data can improve missing mass spectra and other kinematically derived quantities.

6 Kinematic Fit of $\gamma p \to p\pi^+\pi^-\pi^o$

The channel $\gamma p \to p\pi^+\pi^-\pi^o$ provides a good example of how to kinematically fit data in a channel with an undetected particle. We will also use this channel to demonstrate how kinematically fitting data can improve derived kinematic quantities. The setup for this channel is very similar to that of $\gamma p \to p\pi^+\pi^-$. The vector $\boldsymbol{\eta}$ and the covariance matrix C_η are the same as in section 5. We again set $\boldsymbol{y_0} = \boldsymbol{\eta}$, where the η_j's are the measured values of the fit parameters.

To handle the undetected π^o, we set up the vector $\boldsymbol{x}$ according to ,

$$\mathbf{x} = \begin{pmatrix} p_{x_{\pi^o}} \\ p_{y_{\pi^o}} \\ p_{z_{\pi^o}} \end{pmatrix} , \tag{52}$$

where x, y and z are the Cartesian coordinates in the lab system. We construct our initial estimate of the unknown parameters, $\mathbf{x_0}$, out of the total missing 4-momentum. The constraint functions for this channel can then be obtained by adding the energy and momentum of the π^o to (47)-(50).

Using the constraint functions, along with the definitions of $\boldsymbol{y_0}$ and $\boldsymbol{x_0}$, the matrices A and B along with the vector $\mathbf{c}$ are easily obtained from (4)-(6). We can then use (11) and (12) to write the least squares estimates of the deviations in the fit parameters as,

$$\boldsymbol{\xi} = -(A^T C_B A)^{-1} A^T C_B \mathbf{c}, \tag{53}$$

$$\boldsymbol{\delta} = -C_\eta B^T C_B (\mathbf{c} + A\boldsymbol{\xi}) . \tag{54}$$

The improved measurements are again written as $\boldsymbol{y} = \boldsymbol{y_0} + \boldsymbol{\delta}$ and the least squares estimates of the parameters x_j are given by $\boldsymbol{x} = \boldsymbol{x_0} + \boldsymbol{\xi}$. The process is then iterated, substituting the

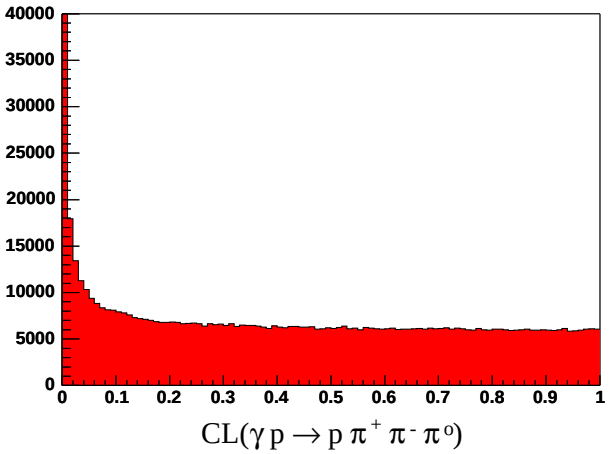

Figure 15: Confidence Level distribution obtained by kinematically fitting the channel $\gamma p \rightarrow p\pi^+\pi^-\pi^o$ (a 1-C fit).

values obtained for $\boldsymbol{y}$ and $\boldsymbol{x}$ in the previous step for $\boldsymbol{y_0}$ and $\boldsymbol{x_0}$ and repeating the calculation. After performing the last iteration, we again use $\boldsymbol{\epsilon} = \boldsymbol{\eta} - \boldsymbol{y}$ to calculate $\boldsymbol{\epsilon}^T C_\eta^{-1} \boldsymbol{\epsilon}$ which follows a χ^2 distribution with 1 degree of freedom. The Confidence Level distribution obtained from this fit can be seen in figure 15. It is important to note here that we have made no missing mass cuts to select out π^o events. We simply fit to the hypothesis that there was a missing π^o, and use the Confidence Level to determine whether this was the case.

We now demonstrate how kinematically fitting data can improve derived kinematic quantities. Figure 16 shows the missing mass off the proton from $\gamma p \rightarrow p\pi^+\pi^-\pi^o$ events before and after fitting. The fit clearly enhances the peaks corresponding to the η and ω mesons (the improvement of the η is quite pronounced, see fig.16b).

Another dramatic affect of kinematic fitting can be seen if we look in the $\gamma p \rightarrow p\omega$ channel. The amplitude for the decay $\omega \rightarrow 3\pi$ can be written as [8],

$$M = M_{JP} M_F \ , \tag{55}$$

where M_{JP} carries the angular momentum and parity dependence and M_F carries the remaining energy-momentum dependence. M_F is approximately constant, yielding,

$$M \propto M_{JP} \ . \tag{56}$$

The ω has $J^P = 1^-$ and decays strongly, therefore, we can write M_{JP} as,

$$M_{JP} \propto \langle 1^- | JP_{3\pi} \rangle \ . \tag{57}$$

The 3π system has negative intrinsic parity, therefore the 1^- piece of the state JP must be in an angular momentum state with $J^P = 1^+$. We can use a J^{th} rank traceless tensor which is symmetric in every pair of indices to describe the angular momentum state J [8]. Clearly, the only 1^{st} rank

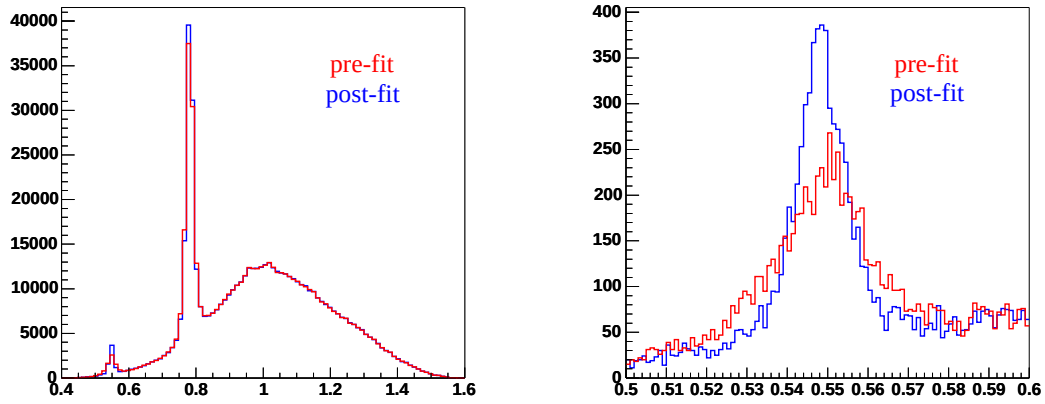

(a) (b)

Figure 16: Missing mass off the proton from $\gamma p \to p\pi^+\pi^-\pi^o$ events before and after kinematic fitting. (b) is a close up of (a) in the η-mass region where the peak in the fit data is clearly enhanced.

tensor with positive parity we can construct is $\mathbf{p}_{\pi_1} \times \mathbf{p}_{\pi_2}$ where π_1 and π_2 are any two of the three decay pions (momenta measured in ω rest frame). Therefore, the probability density of the decay $\omega \to 3\pi$ is given by,

$$\mathcal{P}(\omega \to 3\pi) \propto |\mathbf{p}_{\pi_1} \times \mathbf{p}_{\pi_2}|^2 \, . \tag{58}$$

The maximum value of $|\mathbf{p}_{\pi_1} \times \mathbf{p}_{\pi_2}|^2$ occurs when, in the ω rest frame, the magnitude of all three pions' momenta are equal. We can then define the normalized quantity λ as $|\mathbf{p}_{\pi_1} \times \mathbf{p}_{\pi_2}|^2$ divided by its maximum value. Since the probability density of the decay is linear in λ, a histogram of *events vs.* λ, assuming all pions originate from ω decays, should look like a triangular wedge with zero events at $\lambda = 0$ and reaching a maximum number of events at $\lambda = 1$. Background events, pions that do not originate from an ω decay, produce a flat distribution from 0 to 1 (energy-momentum conservation sets the upper limit on λ at 1, regardless of what type of decay produced the pions). Thus, this gives us an excellent way to calculate the number of ω events and the amount of background present.

Figure 17a shows λ plotted both before and after performing the kinematic fit for the same set of events. The fit result is a dramatic improvement. Kinematic fitting strictly enforces energy-momentum conservation, something that is clearly missing in the pre-fit plot (notice the number of events with $\lambda > 1$).

A more important result can be seen in figure 17b. The red histogram was produced without performing any kinematic fitting and using traditional missing mass cuts. For this histogram, we selected out events with a π^0 by requiring the missing mass off the proton, π^+ and π^- to be between 70 and 210 MeV. We then required the missing mass off the proton to be between 743 and 823 MeV to select out ω events. For the blue histogram we kinematically fit the data and made no missing

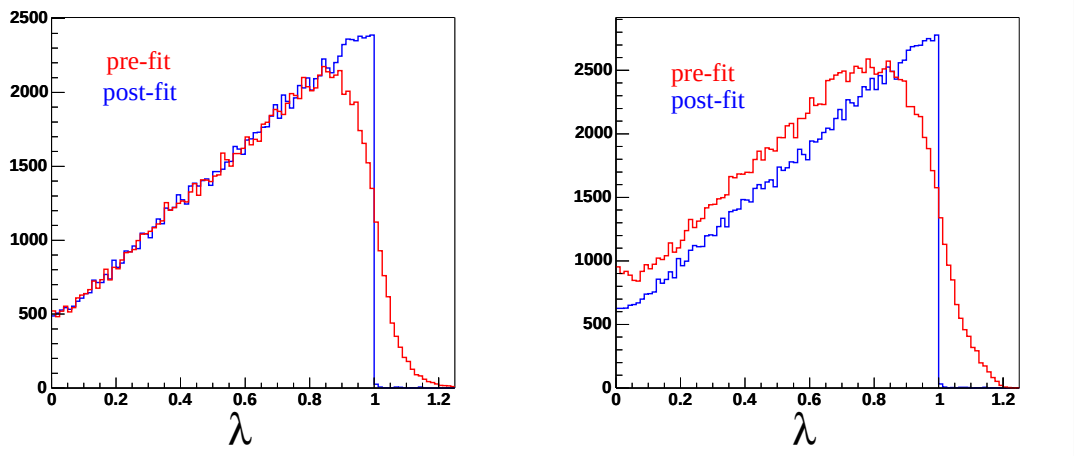

(a) (b)

Figure 17: λ before and after fitting. (a) shows how fitting improves the shape of λ for the same set of events (recall λ should look like a triangular wedge on top of a flat background). (b) shows how using Confidence Level cuts and fit data, not only improves the shape of the distribution, but reduces the background by about 20% compared to selecting events by making missing mass cuts to identify π^o's.

mass cut to select π^0 events. Instead, we required the Confidence Level to be greater than 0.02. We then made the same cut to identify ω events as before, except this time using the missing mass off the proton after fitting. The shape of the λ distribution is again improved, but what's more interesting is that we've eliminated about 20% of the background while losing virtually no signal.

7 Conclusion

We have been able to successfully kinematically fit the channels $\gamma p \to p\pi^+\pi^-\pi^o$ and $\gamma p \to p\pi^+\pi^-$. The Confidence Level and pull distributions obtained from these fits are in good agreement with the theoretical distributions. Kinematic quantities, such as missing mass spectra, calculated from the fit data show significant improvement over those calculated prior to fitting. We have also been able to use kinematic fitting to reduce background in the channel $\gamma p \to p\omega$. The results presented here are for the g1c target. Hopefully, this paper describes the process used to calculate energy loss and multiple scattering effects well enough that it can be repeated for other targets.

References

[1] Siegmund Brandt. *Statistical and Computational Methods in Data Analysis.* North Holland Publishing Company, 1970.

[2] A.G. Frodesen, O. Skjeggestad, and H. Tøfte. *Probablity and Statistics in Particle Physics.* Universitetsforlaget, 1979.

[3] www1.jlab.org/ul/jpix/med/HALB_67.gif

[4] John W.C. McNabb. *Photoproduction of Lambda and Sigma0 Hyperons off Protons in the Nucleon Resonance Region using CLAS at Jefferson Lab*, Ph.D Thesis, Carnegie Mellon University, 2002.

[5] Matthew Bellis, private communications.

[6] Donald H. Perkins, *Introduction to High Energy Physics*, 4th Edition, Cambridge University Press, 2000.

[7] D.I. Sober et al. The bremsstrahlung tagged photon beam in Hall B at JLab. *Nuclear Instruments and Methods in Physics Research A*,440:263-284, 2000.

[8] Charles Zemach. Three-Pion Decays of Unstable Particles. *Physical Review*,133:B1201-B1220, 1964.